Asian Journal of Chemistry; Vol. 32, No. 12 (2020), 3219-3226

ASIAN JOURNAL OF CHEMISTRY

https://doi.org/10.14233/ajchem.2020.23034

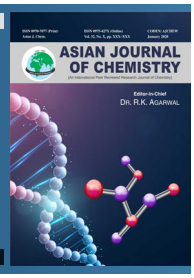

Synergistic Effect of Polyethylene Oxide Layer on TiO_2/TiO_2-Graphene based Perovskite Solar Cell

DEEPIKA GAUR[1], SUNITA SHARMA[1,*], S.K. GHOSHAL[2], POOJA SETH[3], SHRUTI AGGARWAL[3] and NEHA AGGARWAL[4]

[1]Department of Applied Sciences, The NorthCap University, Gurugram-122017, India
[2]Department of Physics, AOMRG, Faculty of Science, Universiti Teknologi Malaysia, Skudai 81310, Johor Bahru, Malaysia
[3]School of Basics and Applied Sciences, Guru Gobind Singh Indraprastha University, Dwarka, Delhi-110078, India
[4]Advanced Materials and Devices, CSIR-National Physical Laboratory, Dr. K.S. Krishnan Marg, New Delhi-110012, India

*Corresponding author: E-mail: sunphotonics@gmail.com

Received: 29 October 2020; *Accepted*: 6 November 2020; *Published online*: 7 December 2020; AJC-20164

This article reports the influence of titania (TiO_2) and TiO_2-graphene (TGr) as electron transport layer (ETL) on the performance of polyethylene oxide (PEO) based perovskite solar cell (PSC). Compared to most commonly used ETLs, graphene based ETLs showed immense promise towards scalable fabrication and higher carrier injection of PSC. Driven by this idea, PEO layer was introduced in TiO_2 and TGr based PSC to inspect the feasibility of achieving notably high fill factor. As-grown nanocomposites were analyzed using varied analytical tools to determine the effect of graphene inclusion on their morphology, optical and electrical properties. An increase in the absorption bandwidth and red-shift in the absorption peak was observed from UV-VIS spectra indicating band gap narrowing. By exploiting TGr nanocomposite in perovskite solar cells as electron collection layer, a remarkable fill factor of 44% has been achieved. In short, present disclosure may contribute towards the development of ETL in high performing PEO based perovskite solar cell (PSC).

Keywords: Perovskite solar cells, Titania, Graphene, Absorption, Photoluminescence, Fill factor.

INTRODUCTION

Of late, organic-inorganic hybrid perovskites solar cells (PSCs) became prospective in the field of photovoltaics [1-5]. Over the years, the efficiency of PSCs has been reported to improve significantly from 3.8% in 2009 [6] to 22.1% [7]. Clearly, in less than three years, the performance of PSCs could achieve a level comparable to those of much more matured thin film solar cell technologies including CdTe and CIGS that consumed few decades to reach similar efficiencies. Amongst all organic-inorganic hybrid perovskite (PVK) materials, $CH_3NH_3PbI_3$ displayed enormous light harvesting capacity that is useful for the design of cost-effective and highly efficient solar cells [8,9]. Furthermore, to enhance the efficiency of PSCs appropriate electrolytes are required in the solar cell structure. The applications of liquid-based perovskite solar cell are limited due to stability issues involving instant dissolution of the perovskite materials in the liquid electrolyte [10]. Thus, several fundamental shortcomings need to be overcome to commercialize PSCs technology in the near future. These issues include: (i) growth and deposition of controllable perovskite thin films, (ii) scalable and reproducible processes, (iii) cells with high stability and long lifetime, and (iv) low toxicity. On top, manufacturing companies must be concerned about the cost of PCSs to become competitive in the market [11]. The volatility and leakage of liquid solvent in PSCs are detrimental for outdoor applications, where robust encapsulations are essential to prohibit such effects [12]. Accordingly, considerable efforts have been made to replace the liquid electrolytes with solid-state electrolyte. For applications in PSCs, ionic conductors have been emerged as promising candidates among the solid-state electrolyte materials [12]. Titania (TiO_2) has predominantly been exploited as electron transport material (ETM) owing to its high chemical and thermal stability, photo-stability, photo-cataliticity, non-toxicity and inexpensiveness [13]. Besides, due to profound energy level match between TiO_2 and perovskite material, titania significantly improves the exciton separation efficiency [14-16]. Lately, graphene and related 2D materials have been introduced in the cells structure in order to improve the charge injection and/or collection at the electrodes, leading to an augmentation in the power conversion efficiency and a long-term stability [17,18]. Particularly, the incorporation of

graphene into the TiO_2 layer led to an enhancement in the efficiency plus stability of both small and large area devices [19]. Despite many dedicated efforts the design of highly efficient PSCs has been limited to the glove-box setting [20]. In short, stable and highly efficient room temperature PSCs are far from being achieved. Inspired by the renewable energy generation prospect of PSCs, an attempt is made to fabricate low-cost and efficient perovskite sensitized solar cells using solid polymer electrolyte with TiO_2 and TiO_2-graphene (TGr) as electron transport material (ETM). To the best of our knowledge for the first time such combinations of materials were utilized in the device structure. The perovskite material ($CH_3NH_3PbI_3$) was synthesized and sandwich structures (PSCs) with indium tin oxide-porous TiO_2 and TGr/perovskite//PEO-KI/I_2//Pt-coated ITO was designed. These PSCs were character-ized using diverse analytical tools to determine their room temperature performance.

EXPERIMENTAL

Analytical grade high purity chemical reagents such as dimethylformamide, Ti(IV) bis(acetoacetato)diisopropoxide, lead iodide, polyethylene oxide (PEO) and hexachloroplatinic acid (H_2PtCl_6), methylamine, hydroiodic acid (55 wt.% in water), petroleum ether, methanol, titanium dioxide, graphene, potassium iodide and iodine were used without further purification.

Synthesis of methylammonium lead triiodide: First, methylammonium iodide (CH_3NH_3I) was synthesized by mixing methylamine and hydroiodic acid in a round bottle flask. Next, the solution was treated in ice-bath (0 ºC) and continuously stirred for 2 h. Then, the resultant product was kept overnight in an oven (60 ºC) for complete vaporization. Later, the precipitate of CH_3NH_3I was collected in a round bottom flask and washed thoroughly using diethyl ether until the appearance of whitish colour. Subsequently, the white precipitate was dried at 80 ºC in hot air oven for 20 h. Meanwhile, methylammonium lead triiodide ($CH_3NH_3PbI_3$) solution was prepared by mixing equimolar ratio (1:1) of CH_3NH_3I and PbI_2 in 2 mL of DMF, wherein the resultant solution was continuously stirred for 6 h at 60 ºC. The achieved solution was used to deposit perovskite thin film for designing the desired solar cell [21,22].

Design of perovskite solar cell (PSC): The ITO-coated glass substrates were cleaned by acetone, ethanol and deionized water each for 30 min in an ultrasonic bath to deposit the perovskite film. The following steps were followed:

Deposition of blocking layer: Initially, a layer of Ti(IV) bis(acetoacetato)diisopropoxide was deposited by spin coating at the revolution of 2000 rpm for 30 s, wherein 0.15 M titanium diisopropoxide bis(acetylacetonate) solution in 1-butanol was utilized. Next, the as-coated film was dried at 125 ºC for 5 min before another layer of the same material being deposited via spin coating at the rotation of 3000 rpm for 30 s. The resultant coating was then dried at 125 ºC for 15 min. Later, a layer titanium diisopropoxide bis(acetylacetonate) solution (0.3 M) was deposited using spin coating at the speed of 2000 rpm for 20 s. Finally, the as-prepared thin film was sintered at 500 ºC for 15 min [23].

Deposition of electron transport layer (ETL): First, a paste of TiO_2/TGr was prepared by mixing PEG and deionized water in a pastel mortar. Then, a thin film of TiO_2/TGr was deposited on the blocking layer by doctor blade method. The coated substrate was sintered at 500 ºC for 30 min using a heating rate of 2 ºC/min followed by cooling at room temperature [24].

Deposition of perovskite layer: A solution of $CH_3NH_3PbI_3$ was spin coated onto the TiO_2 film at the revolution of 1000 rpm for 15 s. Next the film was heated at 70 ºC for 30 min [21,22].

Deposition of PEO based polymer electrolyte layer: The solid polymer electrolyte solution consisting of PEO:KI and I_2 (20% of PEO and 10% of KI) was prepared using methanol as the solvent. Then, the prepared solution was coated as an electrolyte in the PSC using spin coating operated at the speed of 2000 rpm for 20 s [21,22,25].

Deposition of counter electrode layer: Platinum counter electrode (CE) was deposited on conductive glass using ethanolic H_2PtCl_6 solution *via* spin coating. The produced electrode was sintered at 400 ºC for 30 min at heating rate of 4 ºC/min. Fig. 1 displays the designed PSC structure [working electrode (ITO/BL/TiO_2/Gr-TiO_2/Perovskite)//PEO:KI:I_2//CE] [21,22,25]. Two types of devices were prepared using different blends of ETMs to achieve unlike combination of PSC. Table-1 enlists designation and details of the PSC structure depending on ETMs and ETLs. Fig. 2 shows the energy band diagram of PSC.

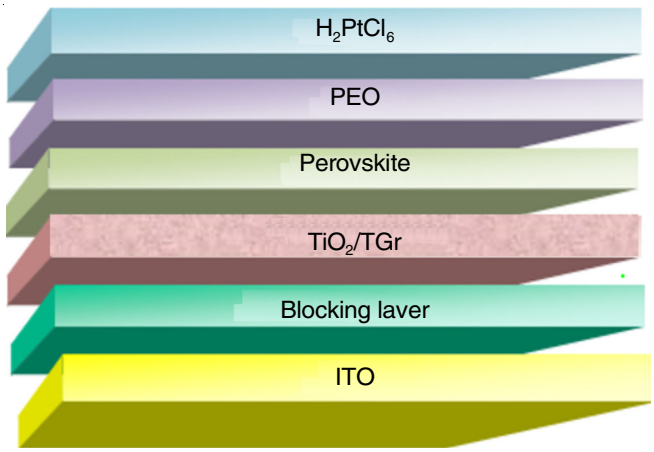

Fig. 1. Structure of designed PSC

Characterization: The crystalline phase and structural properties of prepared samples were studied by using a Bruker D8 Advance X-ray diffractometer with CuKα radiation of wavelength λ = 0.15405 nm. All XRD measurements were

TABLE-1
DESIGNATION AND DETAILS OF THE PSC STRUCTURE BASED ON ETMs AND ETLs

Device	Structure	ETL	ETM
Cell-1	(ITO/BL/TiO_2/Perovskite)//PEO:KI:I_2//CE)	ETL-1	TiO_2
Cell-2	(ITO/BL/TGr/Perovskite)//PEO:KI:I_2//CE)	ETL-2	TGr

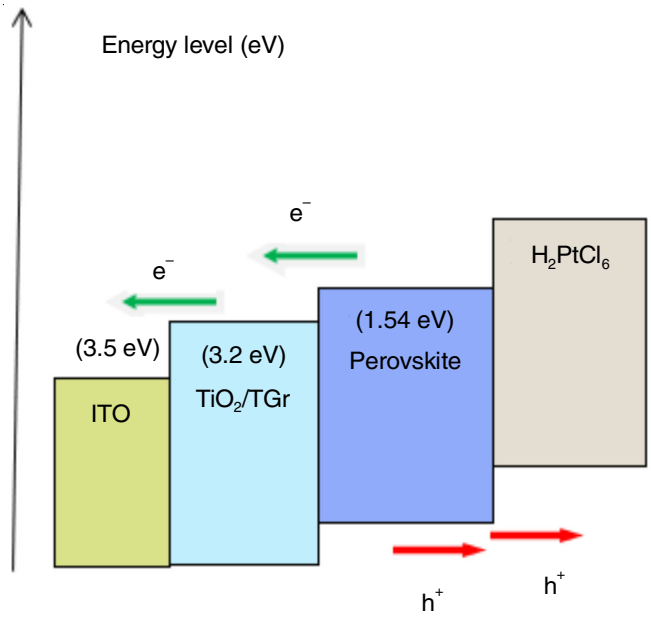

Fig. 2. Energy band diagram of PSC

performed in the range of $2\lambda = 10^{\circ}$-80° at a scan speed of 3°/min at room temperature. The surface morphology of perovskite layer and the designed PSC was examined by Field Emission Scanning Electron Microscope (FE-SEM: MIRA II LMH from TESCAN and High Vacuum Scanning Electron Microscope Emcrafts Genesis -1000). The UV-Vis absorption, reflectance and transmittance spectra of ETL-1, ETL-2, PEO layer, perovskite layer and PSC in the wavelength range of 200 to 800 nm were recorded using UV-Vis-NIR spectrophotometer (Cary 5000). PL measurements of prepared samples at excitation wavelength of 325 nm were conducted *via* LS 55 Photoluminescence spectrometer (Perkin-Elmer). The proposed cells were illuminated by Solar Simulator Model #5550 (1000 W cm^{-2}). All the characterizations were performed at room temperature.

RESULTS AND DISCUSSION

SEM studies: Fig. 3a-d illustrates the SEM images of ETL-1, ETL-2, perovskite layer and PSC. ETL-1 revealed rough and porous morphology with well dispersed TiO_2 particles (Fig. 3a). The morphology of ETL-2 showed the presence of graphene

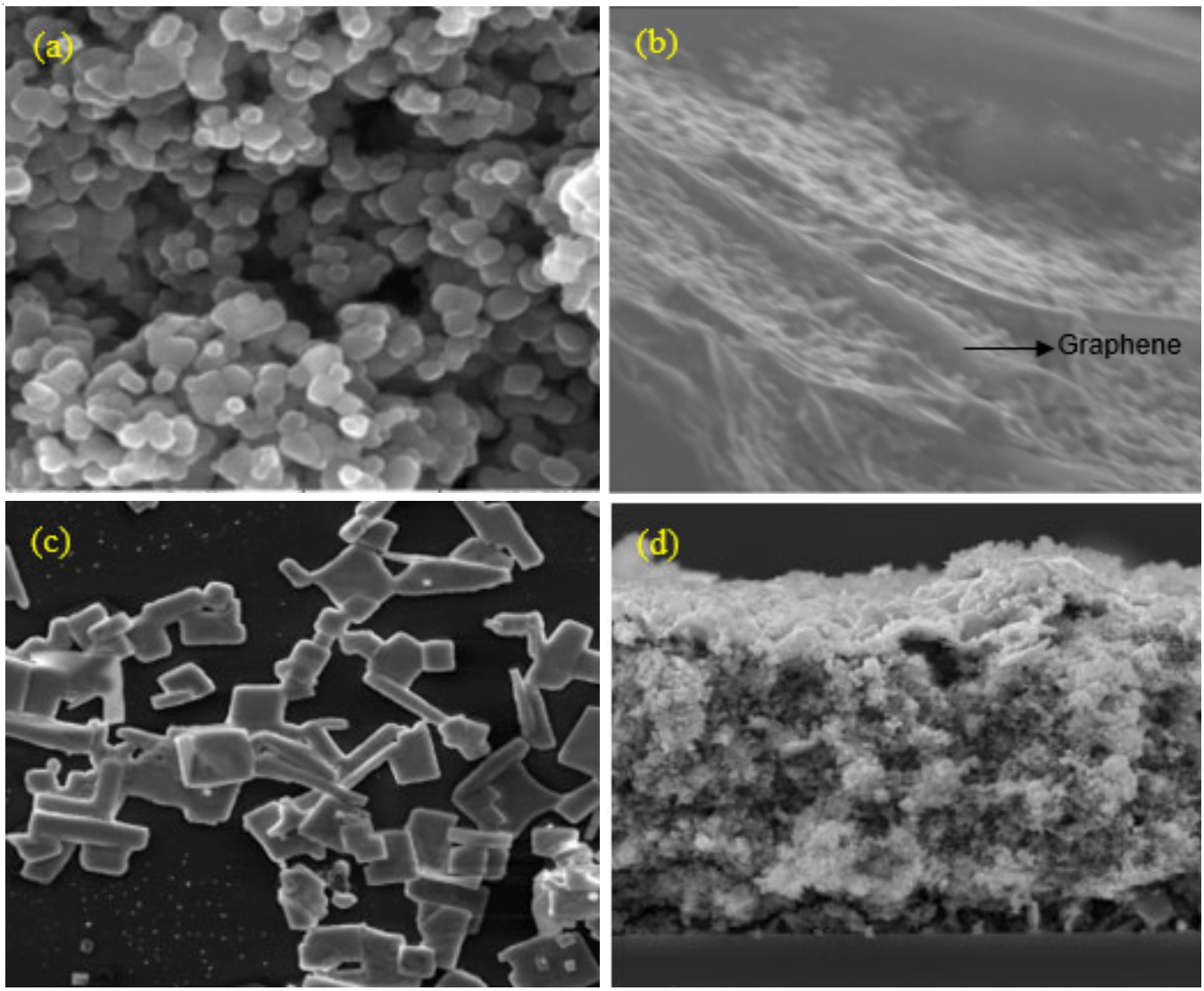

Fig. 3. SEM images of (a) ETL-1 (b) ETL-2, (c) perovskite layer and (d) cross-sectional view of Cell-1

in the form of layered structure (Fig. 3b), verifying the successful incorporation of graphene in TiO_2 [26,27]. The SEM micrograph of perovskite layer displayed to homogeneous dispersion of highly crystalline material particles (Fig. 3c). Besides, the cross-sectional SEM image of Cell-1 (Fig. 3d) disclosed the formation of various layers of BL, ETL, PVK, PEO and H_2PtCl_6 [22,24].

XRD studies: Fig. 4a-b depict the XRD patterns of ETL-1 and ETL-2. The appearance of sharp crystalline peaks at 2θ values of 25.2º, 37.8º, 48.0º, 53.9º and 55.1º were assigned to respective lattice growth orientation along (101), (004), (200), (105) and (211) crystal planes of ETL-1 and ETL-2. The typical diffraction peak belonging to the graphene in ETL-2 was observed at 2θ value of 26.8º [24,28,29]. The XRD data support the SEM results.

Absorption spectral studies: Fig. 5a-b presents the UV-visible absorption spectra of ETL-1, ETL-2, PSC, perovskite- and PEO-layer. The absorption peak of ETL-2 displayed a red shift (Fig. 5a) accompanied by enhanced absorbance due to the incorporation of graphene in TiO_2. Additionally, the observed red shift in the absorption edge of TGr nanocomposite was ascribed to the synergism between semi-metallic graphene and semiconducting titania [28,30-32]. The optical band gap energy (E_g) of ETL-1 and ETL-2 calculated using $E_g = hc/\lambda$ (where h is the Plank constant, c denotes the speed of light, and λ specifies the absorption wavelength) was found to be ≈ 3.06 eV and ≈ 2.89 eV, respectively [33]. It is worth noting that the band gaps of semiconductors being directly related to the range of absorbed wavelength often show narrowing with the increase in the absorption wavelength as reported elsewhere [26]. It was confirmed that TGr incorporated PSC has higher absorbance compared to PEO and PVK layer (Fig. 5b). The absorbance of PVK layer, PSC and PEO layer was observed to be very high in the UV-visible domain (Fig. 5b) where the corresponding peak absorbance were 2.2 (at 316 nm), 3.03 (at 314 nm) and 1.16 (at 319 nm). This clearly indicated that PVK layer and PSC could absorb the majority of the irradiance energy from the solar spectrum.

Fig. 6 displays the reflectance spectra of ETL-1 and ETL-2 in the incident wavelength range of 400-800 nm. The reflectance

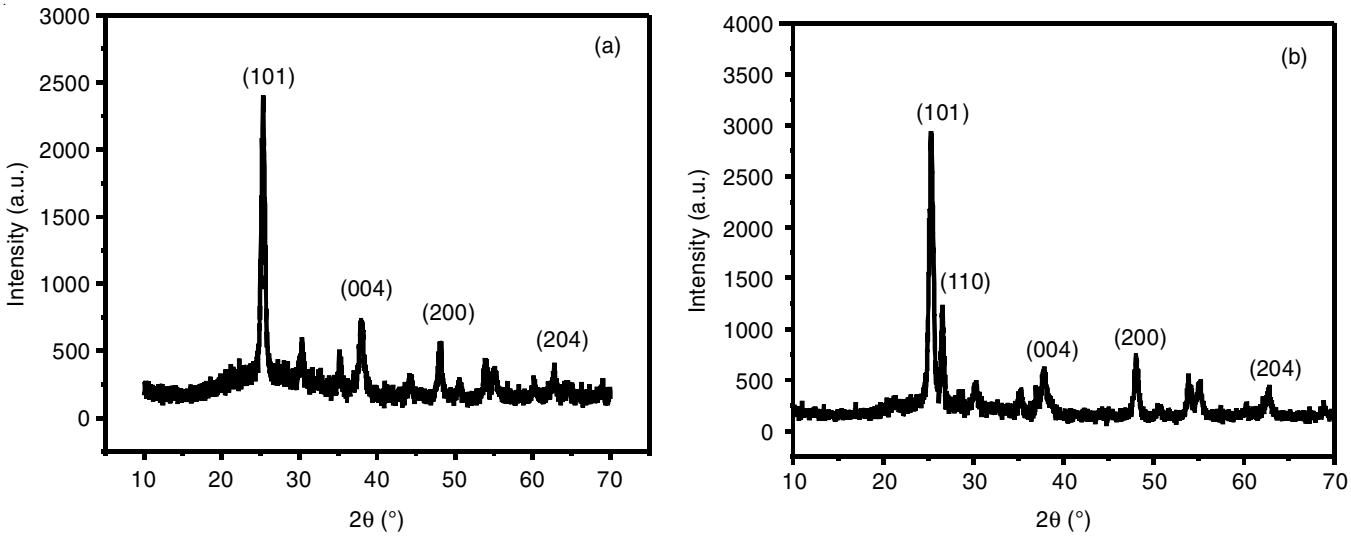

Fig. 4. XRD pattern of (a) ETL-1 and (b) ETL-2

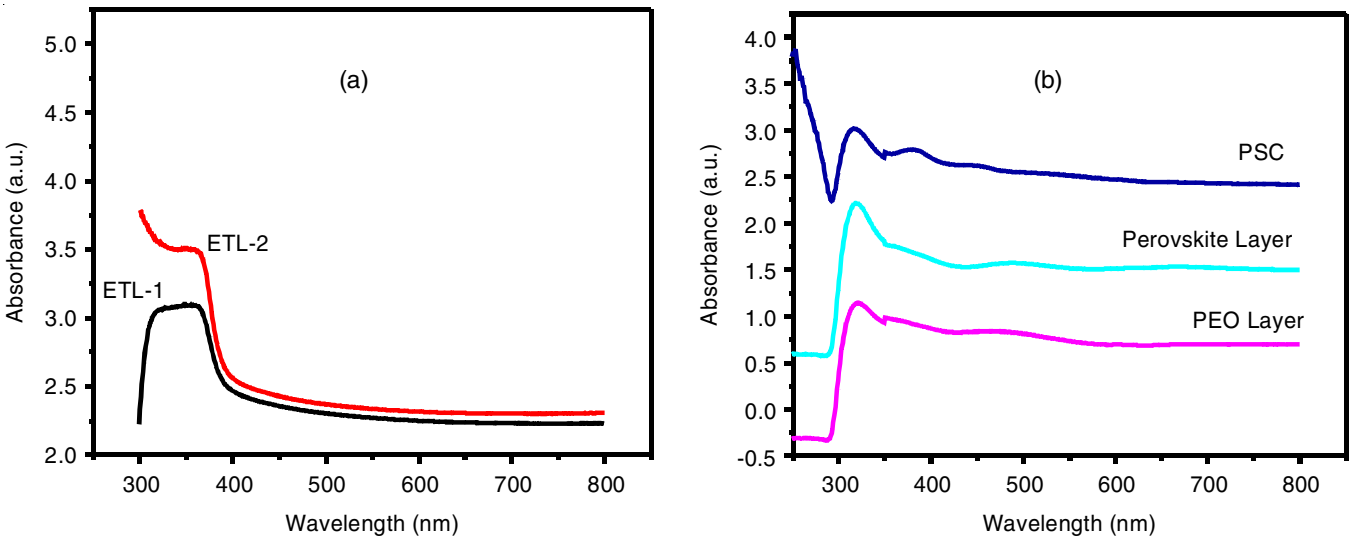

Fig. 5. UV-vis absorbance spectra of (a) ETL-1 and ETL-2 and (b) PSC, perovskite-and PEO-layer

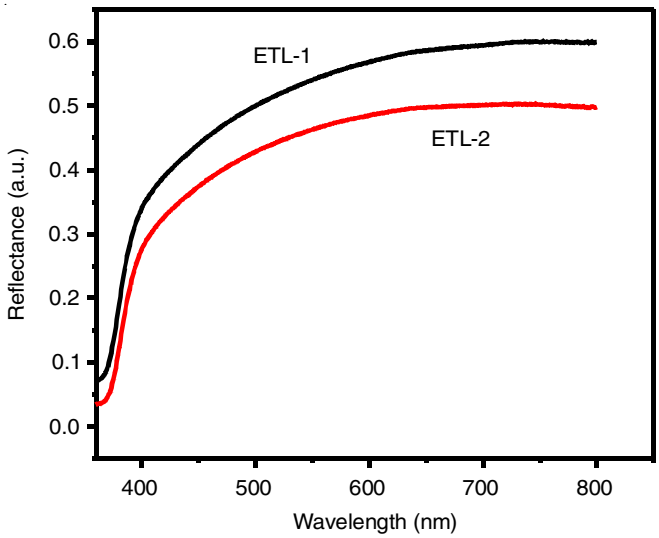

Fig. 6. Reflectance spectra of ETL-1 and ETL-2

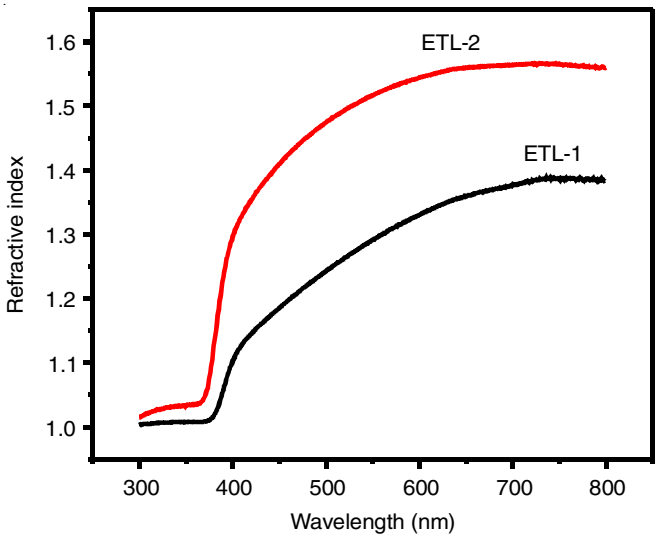

Fig. 8. Refractive index of ETL-1 and ETL-2

of ETL-1 was higher than ETL-2. Fig. 7 shows the transmission spectra of ETL-1 and ETL-2. It was observed that ETL-2 could transmit light more effectively in the UV-VIS-NIR region than ELT-1, which satisfied the foremost requirement to be a good ETL material. The absorption and reflectance data were further used to determine the refractive index (n_f) of ETL-1 and ETL-2. Refractive index in terms of reflectance (R) was expressed as [34]:

$$R = \left(\frac{n_f - 1}{n_f - 1} \right)^2 \tag{1}$$

with

$$n_f = \frac{1 + R + \sqrt{R}}{1 - R} \tag{2}$$

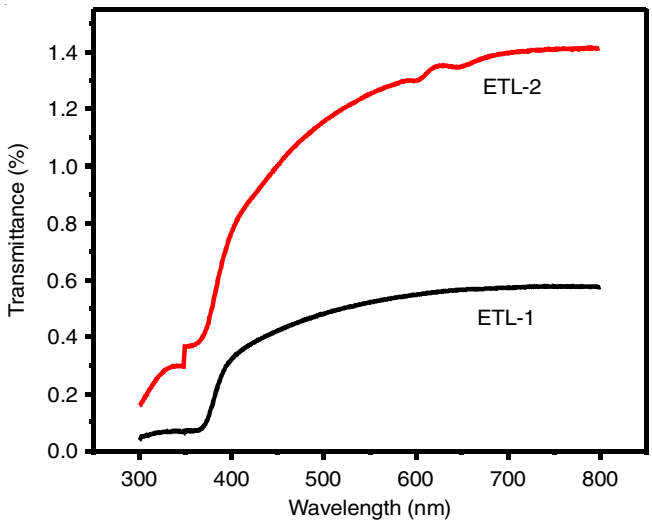

Fig. 7. Transmittance spectra of ETL-1 and ETL-2

Fig. 8 illustrates the wavelength dependent refractive index variation of ETL-1 and ETL-2. The obtained high refractive indices of ETL-2 and ETL-1 were attributed to the normal dispersion traits of the former. These high values of refractive indices signified the strong light scattering capacity of the material with respect to surrounding media. The values of absorbance, reflectance, transmittance, refractive index, and dielectric constant of ETL were somewhat higher than ETL-1. Higher refractive index signifies lower light speed (slowing down due to more light-matter interaction) in the medium, thereby higher absorption. Furthermore, substantially higher transmittance of ETL-2 in the UV-VIS-NIR region than ETL-1 (Fig. 7) confirmed the effectiveness of ETL-2 in the high-performance cell design [34,35].

Fig. 9 shows the variation of the dielectric constant ($k = n^2$) of ETL-1 and ETL-2 as a function of absorption wavelength, a significant parameter for semiconductor device applications. The values of k for ETL-2 were increased after incorporating graphene in TiO_2. Materials with higher dielectric constant have lower exciton binding energies and thus reveal reduced recombination, improving the charge carrier extraction efficiency. It was affirmed that by inserting graphene in TiO_2 the charge carriers' recombination efficiency can be lowered as supported by PL results.

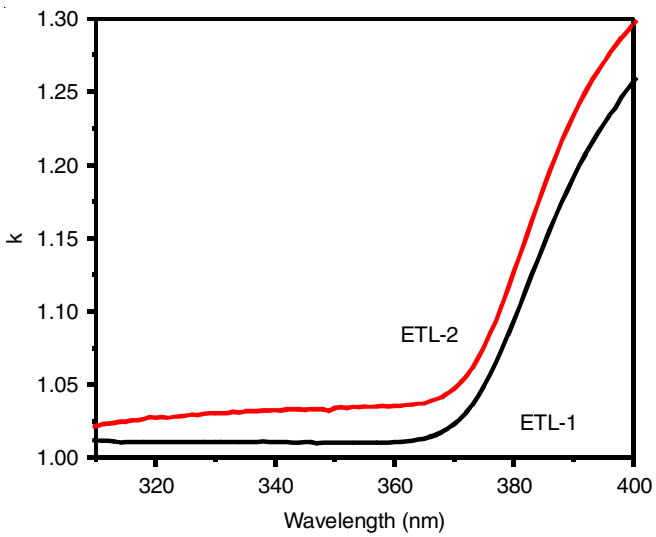

Fig. 9. Dielectric constant of ETL-1 and ETL-2

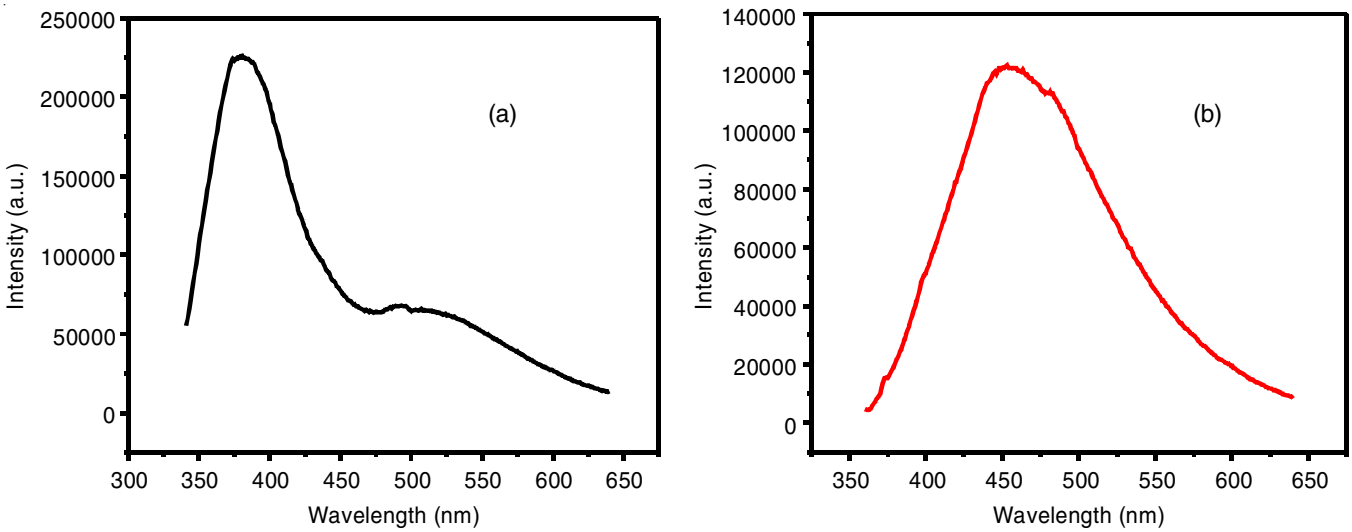

Fig. 10. Photoluminescence (PL) spectra of (a) ETL-1 and (b) ETL-2

Photoluminescence spectra: The room temperature PL spectra (at excitation wavelength of 325 nm) of ETL-1 and ETL-2 (Fig. 10a-b) were recorded to determine the mechanism of photo-generated species. The performance of charge carrier trapping, the recombination of photo-generated charge carriers and the fate of excitons in these materials were determined by analyzing the PL spectral data. The luminescence efficiency of the ETL-1 was higher compared to ETL-2. This clearly indicated that rate of charge recombination in ETL-1 was higher than ETL-2, which was attributed to the occurrences of fast carrier's transport pathways in ETL-2 offered by graphene (2D material) [36,37].

Electrical properties: Figs 11 and 12 displays the current-voltage (I-V) curves of Cell-1 and Cell-2 having respective active area of 0.24 cm^2 and 0.26 cm^2 obtained using solar simulator. The following mechanisms were majorly involved to generate the current [38]:

Process 1: Photoexcitation of perovskite

$$\text{Perovskite} + h\nu \longrightarrow (e^{-}\cdots h^{+})\ \text{perovskite}$$

Process 2: Electron injection

$$(e^{-}\cdots h^{+})\ \text{perovskite} \longrightarrow e^{-}_{cb}\,(TiO_2) + h^{+}\ (\text{perovskite})$$

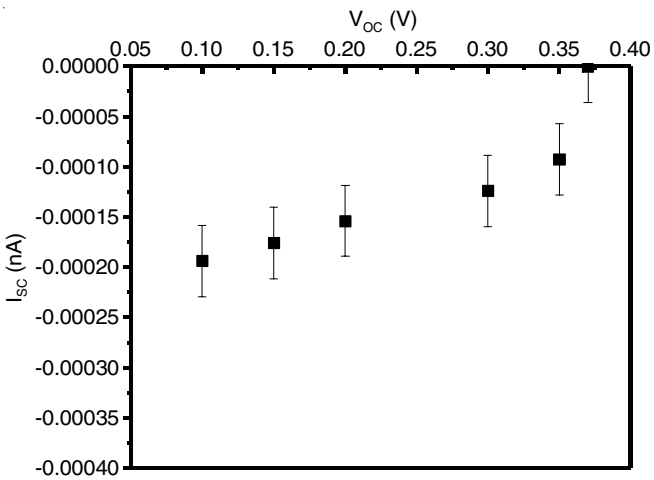

Fig. 11. I-V characteristics of Cell-1

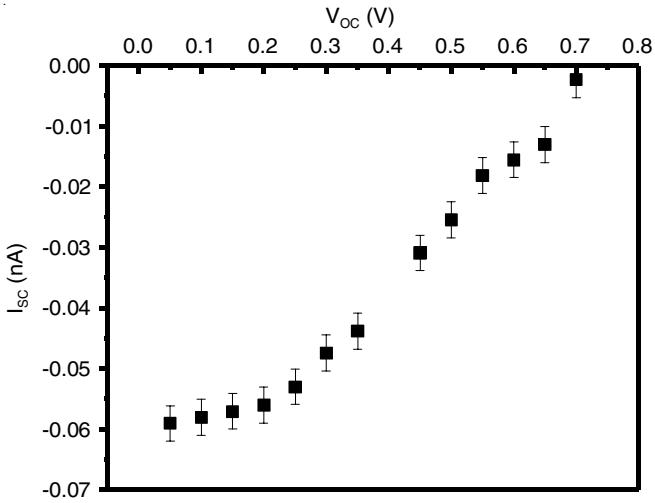

Fig. 12. I-V characteristics of Cell-2

where e^{-}_{cb} is electron in conduction band.

$$h^{+}\ (\text{perovskite}) \longrightarrow h^{+}\ (\text{HTM})$$

Process 3: Hole injection

$$(e^{-}\cdots h^{+})\ \text{perovskite} \longrightarrow h^{+}(\text{HTM}) + e^{-}\ (\text{perovskite})$$

$$e^{-}\ (\text{perovskite}) \longrightarrow e^{-}_{cb}\ (TiO_2)$$

Process 4: Photoluminescence

$$(e^{-}\cdots h^{+})\ \text{perovskite} \longrightarrow h\nu$$

Process 5: Non-radioactive recombination

$$(e^{-}\cdots h^{+})\ \text{perovskite} \longrightarrow \nabla$$

Process 6: Back electron transfer at TiO_2-pervoskite junction

$$e^{-}_{cb}\ (TiO_2) + h^{+}\ (\text{perovskite}) \longrightarrow \nabla$$

Process 7: Back charge transfer at perovskite-HTM junction

$$h^{+}\ (\text{HTM}) + e^{-}\ (\text{perovskite}) \longrightarrow \nabla$$

Process 8: Charge recombination at TiO_2-HTM interface

$$e^{-}_{cb}\ (TiO_2) + h^{+}\ (\text{HTM}) \rightarrow \nabla$$

The overall photovoltaic conversion efficiency of the proposed perovskite cell was controlled through these processes.

TABLE-2
PHOTOVOLTAIC PERFORMANCE OF PSC CALCULATED FROM I-V CURVES

PSC with TiO_2			PSC with TGr		
V_{oc} (V)	I_{sc} (mA)	FF	V_{oc} (V)	I_{sc} (mA)	FF
0.37	1.18×10^{-10}	0.23	0.7	4.7×10^{-8}	0.52

To achieve high PCE, charge generation and transport (Process 1 to 3) must happen at faster rate compared to the undesired recombination (Process 4 to 8). These mechanisms were indeed activated *via* the inclusion of graphene into TiO_2, supporting the implementation of graphene into the cell design [39]. Significant cell parameters including the short circuit current (I_{sc}), open circuit voltage (V_{oc}) and fill factor (FF) were evaluated from the I-V curves (Table-2). Clearly, the FF of Cell-2 containing TGr nanocomposite was 29% higher than Cell-1 that enclosed TiO_2 only. 44% increase in the value of FF in Cell-2 than in Cell-1 using PEO [24,39-41]. Fill factor is a parameter which, in conjunction with V_{oc} and I_{sc}, determines the maximum power from a solar cell so I-V studies shows that Cell-2 to be remarkably better than Cell-1 by using PEO as an electrolyte as there is a significant increase (100 fold) in I_{sc} too.

Conclusion

For the first time, different combinations of TiO_2-graphene (TGr) nanocomposite were used to design organometallic trihalide perovskite solar cells (PSCs). The achieved appreciable reduction in the recombination losses and improvement in the V_{oc}, I_{sc}, and fill factor values were attributed to the synergism between graphene and TiO_2 nanoparticles. Essentially, the formation of energy barriers at the material interfaces was reduced because of graphene′s work function in-between ITO and TiO_2 conduction band, enabling TGr nanocomposite a better electron collector than TiO_2 alone. It was established that TGr nanocomposite could be compatible for reel-to-reel processes required for large scale industrial manufacturing on varied substrates and multilayer architectures. In short, present strategy may open up new avenue for graphene incorporated PSC development. Perovskite solar cells which have potential of becoming an innovative technology for modules, panels and space applications. The present results open a new route to cost-effective and highly efficient perovskite solar cells (PSCs).

ACKNOWLEDGEMENTS

The authors are thankful to Inter University Accelerator Centre, New Delhi, India for providing characterization facilities. Financial support through grant UTM/RU (17H19 and 18H68) is also appreciated.

CONFLICT OF INTEREST

The authors declare that there is no conflict of interests regarding the publication of this article.

REFERENCES

1. W.S. Yang, J.H. Noh, N.J. Jeon, Y.C. Kim, S. Ryu, J. Seo and S.I. Seok, *Science*, **348**, 1234 (2015); https://doi.org/10.1126/science.aaa9272
2. D. Bi, W. Tress, M.I. Dar, P. Gao, J. Luo, C. Renevier, K. Schenk, A. Abate, F. Giordano, J.-P. Correa Baena, J.-D. Decoppet, S.M. Zakeeruddin, M.K. Nazeeruddin, M. Grätzel and A. Hagfeldt, *Sci. Adv.*, **2**, e1501170 (2016); https://doi.org/10.1126/sciadv.1501170
3. M. Saliba, T. Matsui, J.-Y. Seo, K. Domanski, J.-P. Correa-Baena, M.K. Nazeeruddin, S.M. Zakeeruddin, W. Tress, A. Abate, A. Hagfeldt and M. Gratzel, *Energy Environ. Sci.*, **9**, 1989 (2016); https://doi.org/10.1039/C5EE03874J
4. J.-P. Correa-Baena, A. Abate, M. Saliba, W. Tress, T. Jesper Jacobsson, M. Grätzel and A. Hagfeldt, *Energy Environ. Sci.*, **10**, 710 (2017); https://doi.org/10.1039/C6EE03397K
5. W.S. Yang, B.W. Park, E.H. Jung, N.J. Jeon, Y.C. Kim, D.U. Lee, S.S. Shin, J. Seo, E.K. Kim, J.H. Noh and I. Seok, *Science*, **356**, 1376 (2017); https://doi.org/10.1126/science.aan2301
6. S.-H. Turren-Cruz, A. Hagfeldt and M. Saliba, *Science*, **362**, 449 (2018); https://doi.org/10.1126/science.aat3583
7. X.-X. Gao, D.-J. Xue, D. Gao, Q. Han, Q.-Q. Ge, J.-Y. Ma, J. Ding, W. Zhang, B. Zhang, Y. Feng, G. Yu and J.-S. Hu, *Solar RRL*, **3**, 1800232 (2019); https://doi.org/10.1002/solr.201800232
8. Q. Jiang, Y. Zhao, X. Zhang, X. Yang, Y. Chen, Z. Chu, Q. Ye, X. Li, Z. Yin and J. You, *Nat. Photonics*, **13**, 460 (2019); https://doi.org/10.1038/s41566-019-0398-2
9. D. Zhou, T. Zhou, Y. Tian, X. Zhu and Y. Tu, *J. Nanomater.*, **2018**, 8148072 (2018); https://doi.org/10.1155/2018/8148072
10. N.G. Park, *Mater. Today*, **18**, 65 (2015); https://doi.org/10.1016/j.mattod.2014.07.007
11. L. Qiu, L.K. Ono and Y. Qi, *Mater. Today Energy*, **7**, 169 (2018); https://doi.org/10.1016/j.mtener.2017.09.008
12. P.P. Boix, K. Nonomura, N. Mathews and S.G. Mhaisalkar, *Mater. Today*, **17**, 16 (2014); https://doi.org/10.1016/j.mattod.2013.12.002
13. S. Sharma, Bulkesh Siwach, S.K. Ghoshal and D. Mohan, *Renew. Sustain. Energy Rev.*, **70**, 529 (2017); https://doi.org/10.1016/j.rser.2016.11.136
14. Z. Zhan, J. An, H. Zhang, R.V. Hansen and L. Zheng, *ACS Appl. Mater. Interfaces*, **6**, 1139 (2014); https://doi.org/10.1021/am404738a
15. H. Chang, Y.J. Yang, H.C. Li, C.C. Hsu, I.C. Cheng and J.Z. Chen, *J. Power Sources*, **234**, 16 (2013); https://doi.org/10.1016/j.jpowsour.2013.01.113
16. Y. Wang, J. Wan, J. Ding, J.S. Hu and D. Wang, *Angew. Chem. Int. Ed.*, **58**, 9414 (2019); https://doi.org/10.1002/anie.201902984
17. M. Acik and S.B. Darling, *J. Materi. Chem. A*, **4**, 6185 (2016); https://doi.org/10.1039/C5TA09911K
18. A. Agresti, S. Pescetelli, B. Taheri, A.E. Del Rio Castillo, L. Cinà, F. Bonaccorso and A. Di Carlo, *ChemSusChem*, **9**, 2609 (2016); https://doi.org/10.1002/cssc.201600942
19. M. Acik and Y.J. Chabal, *J. Appl. Phys.*, **50**, 070101 (2011); https://doi.org/10.1143/JJAP.50.070101
20. W.-T. Wang, S.K. Das and Y. Tai, *ACS Appl. Mater. Interfaces*, **9**, 10743 (2017); https://doi.org/10.1021/acsami.7b01038
21. H.S. Kim, C.-R. Lee, J.-H. Im, K.-B. Lee, T. Moehl, A. Marchioro, S.-J. Moon, R. Humphry-Baker, J.-H. Yum, J.E. Moser, M. Grätzel and N.G. Park, *Sci. Rep.*, **2**, 591 (2012); https://doi.org/10.1038/srep00591
22. Rahul, B. Bhattacharya and P. K. Singh, *Curr. Nanomater.*, **1**, 171 (2016); https://doi.org/10.2174/2405461502666161209162815

23. G. Lu, F. He, S. Pang, H. Yang, D. Chen, J. Chang, Z. Lin, J. Zhang and C. Zhang, *Int. J. Photoenergy*, **2017**, 2562968 (2017); https://doi.org/10.1155/2017/2562968
24. B. Siwach, D. Mohan, S. Sharma and D. Jyoti, *Bull. Mater. Sci.*, **40**, 1371 (2017); https://doi.org/10.1007/s12034-017-1492-z
25. R. Bhattacharyya, K. Bhanja and S. Mohan, *Int. J. Hydrogen Energy*, **41**, 2847 (2016); https://doi.org/10.1016/j.ijhydene.2016.01.106
26. S.A. Kazmi, S. Hameed, A.S. Ahmed, M. Arshad and A. Azam, *J. Alloys Compd.*, **691**, 659 (2017); https://doi.org/10.1016/j.jallcom.2016.08.319
27. A. Eshaghi and A.A. Aghaei, *Bull. Mater. Sci.*, **38**, 1177 (2015); https://doi.org/10.1007/s12034-015-0998-5
28. Y. Zhang, Z.-R. Tang, X. Fu and Y.-J. Xu, *ACS Nano*, **4**, 7303 (2010); https://doi.org/10.1021/nn1024219
29. V. Štengl, T. Bakardjieva, T.M. Grygar, J. Bludská and M. Kormunda, *Chem. Cent. J.*, **7**, 41 (2013); https://doi.org/10.1186/1752-153X-7-41
30. S. Liu, C. Liu, W. Wang, B. Cheng and J. Yu, *Nanoscale*, **4**, 3193 (2012); https://doi.org/10.1039/c2nr30427a
31. Q. Huang, S. Tian, D. Zeng, X. Wang, W. Song, Y. Li, W. Xiao and C. Xie, *ACS Catal.*, **3**, 1477 (2013); https://doi.org/10.1021/cs400080w
32. T. Lu, R. Zhang, C. Hu, F. Chen, S. Duo and Q. Hu, *Phys. Chem. Chem. Phys.*, **15**, 12963 (2013); https://doi.org/10.1039/C3CP50942G
33. A.A. Madhavan, S. Kalluri, D. K Chacko, T.A. Arun, S. Nagarajan, K.R.V. Subramanian, A.S. Nair, S.V. Nair and A. Balakrishnan, *RSC Adv.s*, **2**, 13032 (2012); https://doi.org/10.1039/c2ra22091a
34. G Benno and K Joachim, Optical Properties of Thin Semiconductor Films, pp 1-11 (2003).
35. P.M. Martins, C.G. Ferreira, A.R. Silva, B. Magalhães, M.M. Alves, L. Pereira, P.A.A.P. Marques, M. Melle-Franco and S. Lanceros-Méndez, *Composites B Eng.*, **145**, 39 (2018); https://doi.org/10.1016/j.compositesb.2018.03.015
36. S. Sadhu and P. Poddar, *J. Phys. Chem. C*, **118**, 19363 (2014); https://doi.org/10.1021/jp5023983
37. G. Yue, X. Ma, W. Zhang, F. Li, J. Wu and G. Li, *Nanoscale Res. Lett.*, **10**, 1 (2015); https://doi.org/10.1186/1556-276X-10-1
38. S. Emami, L. Andrade and A. Mendes, *J. Eng. (Stevenage)*, **1**, 52 (2015).
40. J.T.-Wei Wang, J.M. Ball, E.M. Barea, A. Abate, J.A. Alexander-Webber, J. Huang, M. Saliba, I.M. Sero, J. Bisquert, H.J. Snaith and R.J. Nicholas, *Nano Lett.*, **14**, 724 (2014); https://doi.org/10.1021/nl403997a
40. A. Subramanian, C.Y. Ho and H. Wang, *J. Alloys Compd.*, **572**, 11 (2013); https://doi.org/10.1016/j.jallcom.2013.03.171
41. A. Agresti, S. Pescetelli, B. Taheri, A.E. Del Rio Castillo, L. Cinà, F. Bonaccorso and A. Di Carlo, *ChemSusChem*, **9**, 2609 (2016); https://doi.org/10.1002/cssc.201600942